Elsevier Editorial System(tm) for Continental Shelf Research
Manuscript Draft

Manuscript Number:

Title: Influences of upwelling and downwelling winds on red tide bloom dynamics in Monterey Bay, California

Article Type: Research Paper

Keywords: coastal upwelling; winds; phytoplankton; red tides; USA; California; Monterey Bay

Corresponding Author: Dr. J.P. Ryan,

Corresponding Author's Institution: MBARI

First Author: J.P. Ryan

Order of Authors: J.P. Ryan; Andrew Fischer; Raphael Kudela; James Gower; Stephanie King; Roman Marin III; Francisco Chavez

Influences of upwelling and downwelling winds on red tide bloom dynamics in Monterey Bay, California

John P. Ryan[1], Andrew M. Fischer[1], Raphael M. Kudela[2],

James F. R. Gower[3], Stephanie A. King[3], Roman Marin III[1], Francisco P. Chavez[1]

[1¤]*Monterey Bay Aquarium Research Institute*
7700 Sandholdt Road, Moss Landing, California, 95039 USA
[2]*University of California, Santa Cruz. Ocean Sciences & Institute for Marine Sciences*
1156 High Street, Santa Cruz, CA 95064, USA
[3]*Institute of Ocean Sciences*
P.O. Box 6000, Sidney, B.C. V8L 4B2, Canada

Corresponding author:
John Ryan
Phone: (831) 775-1978
Fax: (831) 775-1620
[¤] Correspondence address
ryjo@mbari.org

Abstract

It has recently been shown that inner shelf waters of NE Monterey Bay, California function as an "extreme bloom incubator", frequently developing dense "red tide" blooms that can rapidly spread. Located within the California Current upwelling system, this open bay is strongly influenced by oceanographic dynamics resulting from cycles of upwelling favorable winds and their relaxation and/or reversal. Different wind forcing causes influx of different water types that originate outside the bay: cold nutrient-rich waters during upwelling, and warm nutrient-poor waters during relaxation. In this study, we examine how the bay's bloom incubation area can interact with highly variable circulation to cause red tide spreading, dispersal and retention. This examination of processes is supported by satellite, airborne and in situ observations of a major dinoflagellate bloom during August and September of 2004. Remote sensing of high spatial, temporal and spectral resolution shows that the bloom originated in the NE bay, where it was highly concentrated in a narrow band along a thermal front. Upwelling circulation rapidly spread part of the bloom, mixing cool waters of an upwelling filament with warm bloom source waters as they spread. Diurnal vertical migration of the dinoflagellate populations was mapped by autonomous underwater vehicle surveys through the spreading bloom. Following bloom expansion, a two-day wind reversal forced intrusion of warm offshore waters that dispersed much of the bloom. Upwelling winds then resumed, and the bloom was further dispersed by an influx of cold water. Throughout these oceanographic responses to changing winds, an intense bloom persisted in sheltered waters of the NE bay, where extreme blooms are most frequently observed. Microscopic examination of surface phytoplankton samples from the central bay indicates that spreading of the bloom from the NE bay and mixing with regional water masses resulted in significantly increased abundance of dinoflagellates and decreased abundance of

diatoms. Similar dinoflagellate bloom incubation sites are indicated in other areas of the California Current system and other coastal upwelling systems. Through frequent bloom development and along-coast transports, relatively small incubation sites may significantly influence larger regions of the coastal marine ecosystems in which they reside.

Keywords: coastal upwelling, winds, phytoplankton, red tides, *Cochlodinium fulvescens*

Regional Index Terms: USA, California, Monterey Bay

1. Introduction

1.1. Environmental setting

The central California Current System (CCS) is highly productive due to wind-driven upwelling of nutrient-rich water (Reid et al., 1958; Ryther, 1969; Barber and Smith, 1981). Monterey Bay, California, the largest open bay along the west coast of the U.S. (Figure 1), lies in the central CCS. Climatological conditions in outer Monterey Bay (MB) show upwelling and associated high productivity between approximately March and November (Pennington and Chavez 2000). Under upwelling favorable (northwesterly) winds, cold filaments are generated at Point Año Nuevo, north of the bay, and at Point Sur, south of the bay (Figure 1), and their advection into MB is a major source of cold, nutrient-rich waters (Broenkow and Smethie, 1978; Breaker and Broenkow, 1994; Rosenfeld et al., 1994). Cold filaments originating from the Año Nuevo upwelling typically flow southward across the bay mouth and bifurcate, such that some water flows offshore and some into the bay (Rosenfeld et al. 1994). This upwelling circulation creates what has been termed an “upwelling shadow”, in which residence time and stratification are enhanced (Graham et al., 1992; Graham, 1993; Breaker and Broenkow, 1994; Graham and

Largier, 1997; Castilla et al., 2002). Distinction of the northern bay during the upwelling season is also evident in nutrient distributions, with these waters having the lowest nitrate and highest ammonium concentrations (Broenkow and Smethie, 1978).

Monterey Bay waters are primarily a mixture of recently upwelled water and warmer, less saline offshore water (Graham and Largier, 1997). These warmer offshore waters enter MB during relaxation / reversal of upwelling favorable winds (Bolin and Abbott, 1963; Broenkow and Smethie, 1978; Rosenfeld et al., 1994; Ramp et al., 2005). Early descriptions of MB seasonal variability identified the period of approximately August through October as the "oceanic period", during which upwelling winds are weaker and more variable, and intrusions of warm waters from the California Current are more frequent (Skogsberg, 1936; Skogsberg and Phelps, 1946). This early description is supported by recent analysis of 20 years of satellite sea surface temperature images, which shows that along the central California coast, warm shoreward intrusions are most frequent during August-October (Stegmann et al., 2006). Warm intrusions can profoundly influence phytoplankton ecology. A warm intrusion during the 2002 oceanic period increased stratification while spreading a dense dinoflagellate bloom from the NE bay, throughout the bay and out into the adjacent coastal ocean (Ryan et al., 2005). A warm intrusion during the 2003 oceanic season created a front in which dense phytoplankton patches were sheared into thin layers (Ryan et al., 2008a). In this study we examine the influences of upwelling / cold intrusion and relaxation / warm intrusion on dinoflagellate bloom dynamics during the 2004 oceanic period.

1.2. Red tides and harmful algal blooms

Recent studies show that NE Monterey Bay frequently experiences extreme "red tide" blooms comprised of dense dinoflagellate populations, particularly during the oceanic season

(Ryan et al, 2008b). Dinoflagellate populations in the NE bay can exhibit strong and persistent diurnal vertical migration (Donaghay et al., 2006), and their lateral advection can rapidly expand blooms (Ryan et al., 2005; Kudela et al., 2008; Rienecker et al., 2008). Coastal upwelling systems host diverse dinoflagellate species, many of which can form Harmful Algal Blooms (HABs; Horner et al.; 1997, Smayda, 2000; Kudela et al., 2005). Because dinoflagellates comprise about 50% of all red tide species and 75% of all HAB species (Sournia, 1995; Smayda, 1997), understanding their bloom incubation sites (Ryan et al., 2008b) and mechanisms of spreading is central to advancing understanding and prediction of red tide and HAB phenomena. Among the challenging aspects of dinoflagellate ecology research is investigation of the physical oceanography underlying dinoflagellate bloom development in complex, rapidly changing coastal environments (Tester et al., 1991; Franks and Anderson, 1992; Anderson, 1995; Donaghay and Osborn, 1997; Smayda, 2002; Ryan et al., 2005; Pitcher and Nelson, 2006; Fawcett et al., 2007).

1.3. Research Objectives

The primary objective of this study is to illustrate how responses of ocean circulation to characteristic variability in wind forcing can influence the dynamics of intense dinoflagellate blooms in Monterey Bay, California. Clearer understanding of important processes in one region will support comparative approaches to understanding blooms across different coastal upwelling regions having similar atmosphere-ocean coupling and ecosystem structure. Our approach is integration of intensive multi-scale, multidisciplinary observations.

2. Methods

2.1. Satellite Remote Sensing

Data from two satellite sensors were used in this study. One was the Moderate Resolution Imaging Spectroradiometer (MODIS) on the Aqua satellite. From the MODIS image data we produced true color, chlorophyll fluorescence line height (FLH), chlorophyll concentration, and sea surface temperature (SST) images. We processed MODIS data from Level 1A using the SeaDAS software, applying calibrations for ocean remote sensing developed by the MODIS Ocean Biology Processing Group. The true color images use the 645 nm (red), 555 nm (green) and 469 nm (blue) bands, having spatial resolutions of 250, 500 and 500 m, respectively, with application of a basic atmospheric scattering correction. For the atmospheric correction required to derive products (FLH, chlorophyll and SST), we computed true 250-m aerosol retrievals using the 859 nm band and a fixed aerosol model (Franz et al., 2006). Resulting image data were mapped to a cylindrical projection. The true resolution of FLH, chlorophyll and SST images are at best ~ 1 km at nadir; bilinear interpolation was used to generate 500 m resolution images. The MODIS chlorophyll algorithm consistently failed where the bloom was most intense, but the FLH algorithm (Letelier and Abbott, 1996) provided consistent coverage of the bay, including the most intense regions of the red tide bloom. Further, the FLH patterns closely matched the patterns of reddish coloration evident in the MODIS true color images. Therefore, we present true color, FLH and SST imagery to describe bloom evolution. The second source was full-resolution (300 m) data from the Medium Resolution Imaging Spectrometer (MERIS). Specifically, we used the Maximum Chlorophyll Index (MCI), a particularly effective indicator of intense phytoplankton blooms (Gower et al., 2005).

2.2. Airborne Remote Sensing

Airborne remote sensing of Monterey Bay was acquired during the early stages of bloom expansion. The Airborne Visible/Infrared Imaging Spectrometer (AVIRIS) (Asner and Green, 2001) and the MODIS Airborne Simulator (MAS) (King et al., 1996) were flown on a NASA ER-2 high-altitude (20 km) aircraft on August 26, 2004. Pixel size of the AVIRIS (MAS) images was ~17 (34) m. AVIRIS swath width at this altitude was 11 km, requiring multiple, parallel, overlapping swaths to image the bay. The northern bay was imaged by two adjacent swaths acquired in ~ 27 minutes. The MAS swath width (37 km) permitted imaging most of the bay during each overpass. AVIRIS imagery was atmospherically corrected using an algorithm developed for hyperspectral remote sensing (Gao et al., 2000). Having contiguous 10 nm bands, AVIRIS enabled imaging of bloom intensity by detection of spectral shifts in the ocean surface reflectance peak near 700 nm that are associated with intense blooms (Gower et al., 2005, Schalles, 2006, Dierssen et al., 2006). Ocean color and thermal imagery were derived from MAS data. SST was computed from the at-sensor radiance using the MAS 11.03 micron channel and the emissivity function in the ENvironment for Visualizing Images (ENVI) software. The resulting SST images were calibrated with concurrent SST data from the moorings (Figure 1). We computed a bloom index (BI), similar to the MCI index of MERIS, from MAS at-sensor radiance data (next section).

2.3. Multi-spectral Remote Sensing Algorithms

All multispectral ocean color algorithms used in this study quantify bloom intensity from upwelling radiance in the red – near infrared (NIR) region of the spectrum. The peak in this region of the spectrum can occur between ~685 and 710 nm, depending on the concentration and type of phytoplankton and other particulate and dissolved constituents, and it shifts to longer

wavelengths with increasing bloom intensity (Gower et al., 2005, Schalles, 2006, Dierssen et al., 2006). The methods of deriving bloom imagery are illustrated in Figure 2. Centers of the radiance measurement bands used for each sensor (triangles) are shown relative to reflectance spectra measured in phytoplankton-dominated waters of Monterey Bay. Bloom intensity was quantified as the amount that upwelling radiance in the center band exceeded a linear baseline derived from radiance measured in the adjacent bands. Linear baseline and peak line height are shown for the MAS bands applied to the spectrum from the higher chlorophyll waters. The linear baseline method is well established for both MODIS (Letelier and Abbott, 1996) and MERIS (Gower et al., 2005). The primary difference is that the MODIS fluorescence line height (FLH) center band at 673-683 nm is placed to measure algal chlorophyll fluorescence emission, whereas the MERIS maximum chlorophyll index (MCI) center band at 709 nm is placed to measure strong reflectance in the NIR caused by extremely dense surface accumulations of phytoplankton. Because the airborne MAS sensor does not have a chlorophyll fluorescence band, but does have a band centered in the NIR, the algorithm results in an "extreme bloom" characterization similar to MERIS MCI.

2.4. Moorings

Two moorings, one at the mouth of Monterey Bay (M1) and the other in northern shelf waters (M0) monitored oceanographic and atmospheric variation (Figure 1). The observations include winds at M1, water velocity at both moorings, and salinity and chlorophyll fluorescence at M0. Surface wind speed and direction were measured by a RM Young model 05103 wind monitor. Temperature and salinity were measured by Sea-Bird microcat conductivity, temperature, depth (CTD) sensors at 3.5, 10, 20, 40, and 60 m. Chlorophyll fluorescence at 2 m was measured by a WetLabs backscattering and fluorescence sensor, and sensor readings were

calibrated using extracted chlorophyll measurements of water samples taken next to the sensor regularly during the study period. Water velocities at M0 and M1 were measured by RD Instruments Workhorse acoustic Doppler current profiler (ADCP) instruments. Because shallow circulation transported the bloom, we examined only velocity above 20 m at both locations. The shallowest ADCP velocity measurements at M0 (M1) are at 10 (20) m.

2.5. Autonomous Underwater Vehicle

The MBARI AUV *Dorado* was deployed during the period of bloom expansion, surveying repeatedly from the inner northern shelf to the mouth of the bay and crossing the region from which the dinoflagellate bloom spread. The speed of the AUV during surveys was ~1.5 m s^{-1}, and the vehicle pitch through a sawtooth sampling pattern was 30°. These sampling attributes provided synoptic high-resolution sections through shelf waters. The AUV was equipped with a sensor suite for measuring physical, chemical and optical properties. We present observations from three sensors: a SeaBird SBE 25 CTD that measured temperature and conductivity, a Paroscientific 8CB/4000-I pressure sensor, a HOBI Labs HS-2 sensor that measured optical backscattering at two wavelengths and chlorophyll fluorescence, and an in situ ultraviolet spectrophotometer (ISUS) sensor that measured nitrate concentrations (Johnson and Coletti, 2002).

2.6. Phytoplankton

As part of a long-term monitoring program, surface phytoplankton samples have been collected approximately every three weeks since 1989 at stations C1 and M1 (Figure 1). Enumeration was done on glutaraldehyde-preserved samples of surface whole water filtered onto Poretics, polycarbonate, 0.2um pore size, 25mm diameter membranes. Prepared slides were analyzed under epifluorescence microscopy using a Zeiss Axiophot microscope, and

phytoplankton were identified to functional group at a minimum and to species for the more abundant organisms. Biomass estimates (carbon per liter) were computed for dinoflagellates and diatoms. Cell volume estimates were made from measurements of cell density (counts), dimensions and shape, using equivalent standard geometric shapes. Conversion to carbon used the equations of Eppley et al. (1970): [$\log_{10}$ C = 0.94 $\log_{10}$ Volume – 0.6] for dinoflagellates and [$\log_{10}$ C = 0.76 $\log_{10}$ Volume – 0.29] for diatoms (Buck et al., 1996, 2005).

3. Results

3.1. Bloom Period Overview

The red tide bloom that is the focus of this study caused the strongest bio-optical signal measured at mooring M0 (location in Figure 1) during 2004. Near-surface chlorophyll concentrations increased by a factor of 3 to 4 at this location during late August through early September (Figure 3a). This increase in biomass occurred in two peaks within a 12-day period. Between the two peaks, the rapid decline and rise in chlorophyll concentrations corresponded with a similar pattern in salinity, with an approximately 1-day lag (salinity leading). Through this period of rapid changes in chlorophyll and salinity, winds varied from upwelling favorable (from the NW, 8/24 to 8/28), into a strong wind relaxation / reversal (8/28 to 8/30), and back to upwelling favorable (8/31 to 9/5). As remote sensing and in situ observations show, this wind forcing had profound influences on the development of a major red tide bloom. This bloom will be examined through three phases: expansion, dispersion and retention.

3.2. Bloom expansion

Extreme bloom conditions were observed by two satellite sensors in NE Monterey Bay on August 25, 2004 (Figure 4a). The exceptionally high MERIS MCI signal of this bloom patch

indicates very high near-surface chlorophyll concentrations. Model studies indicate that an MCI value of 2 corresponds with surface chlorophyll concentrations of ~ 400 μg l^{-1} (Unpublished results using model described in Gower et al., 2005). Although this bloom patch was not directly sampled, extracted surface chlorophyll concentrations exceeding 500 μg l^{-1} have been repeatedly measured in dinoflagellate blooms in this area of the bay (Ryan et al., 2008b), and values exceeding 1000 μg l^{-1} were measured in a 2006 bloom (Kudela, unpublished data). The MODIS true color image shows reddish brown discoloration of surface waters in the bloom region (Figure 4a). Recently upwelled water offshore of the bloom patch is evident as the cool SST patch in the outer northern bay (Figure 4a). At that time, southern Monterey Bay exhibited low FLH.

The strong bloom was still present in the NE bay on August 27, as evidenced by the reddish color of surface waters and high FLH (Figure 4b). The major change over this two-day period was the appearance of reddish waters with high FLH in the southern bay. Outer bay currents (Figure 4a,b) were of sufficient magnitude to have transported bloom waters from the northern to the southern bay, a maximum distance of ~ 25 km, during the two days. The satellite image of August 27 (Figure 4b) coincided with a period of gradually decreasing salinity and rapidly increasing chlorophyll concentrations at mooring M0 (Figure 3a), consistent with advection of a salinity gradient and bloom waters past the mooring.

Although no clear satellite imagery of Monterey Bay was acquired on August 26, during a critical stage of the bloom expansion (Figure 4a,b), airborne remote sensing on this day observed structure and transport of the bloom (Figure 5). High-resolution SST more clearly showed the upwelling filament extending across the mouth of the bay from the north, and the sharp SST front of ~ 2°C between the upwelling filament and warm waters of the northern bay

(Figure 5a). The cool waters were evidently flowing into the central bay in a cyclonic circulation over the northern bay, evident in the mooring currents and SST pattern. The bloom index (BI), which accentuates extreme bloom conditions (Figure 5b), showed the highest bloom signal in the NE bay (Figure 5b), where the bloom had been observed by MODIS and MERIS the previous day (Figure 4a). The band of highest BI was along a thermal front (Figure 5). By August 26, some of the most intense bloom was advected seaward and southward (label P in Figure 5b). This patch was connected to the bloom source region by a thin filament of enhanced BI (label F in Figure 5b). The inshore bloom patch was in the warmest waters of the bay, the offshore patch was also in warm waters, and warm filaments extended between the patches (Figure 5a,b). These patterns indicate that warm bloom waters of the NE bay were transported offshore and entrained southward along the flank of the upwelling filament.

AVIRIS hyperspectral imaging showed that much of the advecting bloom exhibited a spectral peak in bands centered at 701 and 711 nm (inset of Figure 5b). Chlorophyll concentrations and remote sensing reflectance spectra measured in situ during a different bloom (Figure 2) showed spectra peaking at 700 nm in waters having chlorophyll concentrations exceeding 50 $\mu g\ L^{-1}$. Thus the regions of the bloom exhibiting a spectral peak in the 711 nm band likely contained chlorophyll concentrations significantly higher than 50 $\mu g\ L^{-1}$, as indicated by the very high MCI corresponding to ~400 $\mu g\ L^{-1}$ (Figure 4a).

In addition to the most concentrated patches, moderate BI values were evident over much of the northern bay and extending into the southern bay (Figure 5b). This signal extended further south in the outer bay, consistent with southward advection of bloom waters and mixing with the upwelling filament that was evidently flowing into the bay (Figure 5a). Airborne images of the bay acquired one hour apart illustrate mixing of the advected bloom with recently upwelled

waters (Figure 6). During this brief period, the nearshore bloom patch and the warmest waters moved northward and onshore (arrow 1 in Figure 6a-d). Concurrently, the warm bloom patch adjacent to the upwelling filament moved southward (arrow 2). The changes in SST around the offshore patch indicate that strong mixing occurred between the warm waters flowing seaward from the inner bay and the cool, recently upwelled waters (arrow 2 in Figure 6a,c).

The AUV surveys across the northern bay on August 26-27 mapped the transport of warm bloom waters. Because the night-time survey was south of the daytime survey (Figure 5a), and shallow transport over the outer bay was southward, the AUV sampling was quasi-Lagrangian, providing the opportunity to sample the same bloom patch. Southward transport of warm waters inshore of the upwelling filament is evident as the expanded domain of shallow, warm water between the first and second transects (15 and 16°C isotherms in Figure 7 a,c). The bloom is defined by chlorophyll fluorescence exceeding the 75^{th} percentile of all measurements from the two surveys (shaded areas in Figure 7). During the day, chlorophyll fluorescence was highest near the surface, within the shallow, warm, low-nitrate waters (Figures 7 a,b). During the night of August 26/27, the bloom was below the warm surface layer, in waters of higher nitrate concentration (Figures 7 c,d). Non-photosynthetic quenching of fluorescence would result in the opposite pattern, with reduced (enhanced) fluorescence at the surface during daytime (nighttime). Further, optical backscatter exhibited the same pattern as chlorophyll fluorescence (not shown). This change in the vertical distribution of phytoplankton, with downward displacement of the population at night into colder, more nutrient-rich water, is consistent with the migratory behavior of dinoflagellates, which can swim into the nutricline during the night for nutrient uptake (Cullen and Horrigan, 1981, Heaney and Eppley, 1981, Donaghay et al., 2006).

3.3. Bloom dispersion

By August 31, the distribution of the bloom had changed significantly. Following the wind reversal (Figure 3b), flow into the bay from the south brought relatively chlorophyll-poor waters, which flushed and mixed with bloom waters in nearly the entire southern bay, extended into the northern bay, and forced bloom waters out of the northern bay (Figure 4c). The patches of high FLH still exhibited a reddish brown color (Figure 4c). Northward flow continued through September 1, bringing cool waters from the Point Sur upwelling into the southern bay (Label 1 in the SST image of Figure 4d). Flow at both moorings was onshore. Weak upwelling had resumed the previous day (Figure 3b), and SST indicated flow of cool, recently upwelled waters into the northern bay (Label 2 in Figure 4d). These flows further dispersed the bloom. A bloom patch flushed from the bay is identified by label 3 in Figure 4d. By September 3, flow at the moorings remained onshore and turned southward at M0, and flow of cold upwelled waters into northern bay further dispersed the bloom (Figure 4e). Outside the bay, the upwelling filament flowed offshore, characteristic of the bifurcated flow of upwelling filaments (Rosenfeld, et al., 1994). The bloom patch flushed from the bay advected southward and was reduced in magnitude (Label 3 in Figure 4e). Observations from mooring M0 showed the hydrographic and bio-optical changes associated with the flushing and mixing. Chlorophyll concentrations and salinity dropped precipitously on August 31 – September 1 when the lower salinity, chlorophyll-poor offshore waters arrived at the mooring site (Figure 3a).

3.4. Bloom retention

While most of the bay exhibited relatively low FLH following bloom dispersion and the return of upwelling, an intense bloom patch was retained in nearshore waters of the NE bay. This patch appeared ruddy brown in the MODIS true color image and exhibited high FLH and

MCI (Figure 4e).

3.5. Phytoplankton community changes

Previous studies have examined dinoflagellate species data from northern bay samples during summer and fall of 2004 (Curtiss, 2008; Kudela et al., 2008). Here we present previously unreported dinoflagellate and diatom data from the central bay (stations C1 and M1, Figure 1) that are relevant to understanding influences of the dinoflagellate bloom dynamics (Table 1). Samples were acquired on August 17, preceding bloom expansion, and September 8, following bloom dispersion. Dinoflagellates dominated biomass on August 17 by a factor of 2. Following bloom expansion and dispersion, dinoflagellate dominance increased to a factor of 49. *Pseudo-nitzschia* species dominated diatom biomass on August 17, and their absence in samples from September 8 accounted for the sharp decrease in diatom biomass.

4. Discussion

4.1. The upwelling shadow

The “upwelling shadow” in northern Monterey Bay is of particular relevance to the observed bloom dynamics. Upwelling shadows strongly influence patterns of water mass distributions, fronts, and circulation, thereby determining distributions of nutrients and plankton (Graham and Largier, 1997, Castilla et al., 2002, Narvaez et al., 2004). One influence is the cyclonic circulation that develops within northern MB during upwelling. This circulation entrained part of the bloom and transported it alongside an upwelling filament, which spread the bloom southward. Another influence of the upwelling shadow is retention. Retention was evident during two phases of the bloom. The first phase was bloom expansion. Despite the strong cyclonic flow transporting part of the bloom seaward and southward, a large patch of the

bloom remained in the NE corner of the bay. This is the same area where drifter studies have indicated a strong retention zone (Ryan et al., 2008b). The second phase of retention occurred when much of the bay was flushed by two water masses: warm offshore waters followed by cold upwelled waters. Data from two satellite sensors on September 3 confirmed that red tide waters were retained in the northernmost upwelling shadow while most of the rest of the bay had been dramatically changed by these water mass influxes. The NE bay thus functioned not only as the source region for the expanding bloom, but also as a refuge from dispersion.

4.2 Bloom transport and water mass mixing

The SST changes observed within the bloom patch as it was entrained by the upwelling filament and transported southward indicate significant mixing of bloom waters with recently upwelled waters. Thus the bloom was not only transported, but also presumably fertilized by relatively nutrient-rich upwelled waters. The high-resolution remote sensing indicated that cross-frontal mixing extended along much of the front, including the northernmost region where it is dominated by buoyancy, and the southern portion dominated by shear (Graham and Largier, 1997). High-resolution SST showed that lateral mixing was stronger in the central and southern bay, i.e. along the southern, shear-dominated portion of the front and where influx of recently upwelled waters into the bay was greatest. The more diffuse bloom patterns in the central and southern bay were consistent with relatively strong cross-frontal and cross-shelf mixing.

4.3. Biological-physical interactions

Dinoflagellate blooms in NE Monterey Bay can form extremely dense populations aggregated near the surface. The great intensity of blooms in this region is related to not only favorable growth conditions for dinoflagellates, but also concentration of populations by biological-physical interactions (Ryan et al., 2008a). A key physical process is convergent

surface flow. Dinoflagellate populations transported into convergent frontal zones can be concentrated if their upward swimming is sufficient to overcome downwelling in the convergence (Ryther, 1955; Franks, 1997; Stumpf et al., 2008). This process is indicated by high resolution remote sensing and in situ observations of blooms in the NE bay (Ryan et al., 2005; Ryan et al., 2008b). In the present study, as the bloom was being transported, it was highly concentrated along a thermal front. The frontal zone extended across waters influenced by the intruding upwelling filament into the warmest waters containing the bloom. The intruding filament flowed toward the bloom and northern shore, consistent with forcing of convergence in the bloom area. Thus, the same physical dynamics that were stirring regional water masses and spreading the bloom probably generated the front in which the bloom was highly concentrated. Bloom concentration, in turn, may have also intensified the front. The spatial coincidence of the most intense bloom patch with the warmest waters indicates that the bloom may have intensified shallow light absorption and heating, a process that can be significant in coastal waters (Dugdale et al., 1987; Cahill et al., 2008).

Interaction between the ecophysiological characteristics of bloom populations (Smayda, 1997) and the physics of bloom transport are also evident in this study. *Akashiwo sanguinea*, *Ceratium spp.*, and *Cochlodinium fulvescens* dominated this bloom, and these phytoplankton have consistently dominated blooms observed in this region (Ryan et al., 2005; Kudela et al., 2008; Curtiss et al., 2008). These phytoplankton are of the “mixing-drift” type (Smayda, 2000; 2002), which are adapted to dynamic and rapidly changing conditions forced by variability in coastal upwelling, including the high velocity zones of fronts, entrainment by coastal currents and responses to wind relaxation. The intensification of dinoflagellate dominance in central Monterey Bay following bloom expansion, dispersion and mixing indicates that the species

comprising the bloom were successfully adapted to energetic environmental variability, as is characteristic of mixing-drift phytoplankton.

4.4. Other coastal upwelling regions

The GEOHAB (Global Ecology and Oceanography of Harmful Algal Blooms) program espouses a comparative approach to studying HAB ecology, in which natural events are compared and contrasted within and between regions to elucidate common forcing mechanisms as well as regionally distinct influences (GEOHAB, 2005; Anderson et al., 2005; Kudela et al., 2008). There is growing evidence of bloom incubation in sheltered regions of coastal upwelling systems, including northern San Louis Obispo Bay on the California coast (*M. Moline*, personal communication), Lisbon Bay on the Iberian coast (*Moita et al*., 2006), Paracas Bay in the Peru upwelling system (Kahru et al., 2004), and St. Helena Bay in the southern Benguela upwelling system (Pitcher and Nelson, 2006; Fawcett et al., 2007). Of these locations, perhaps the most thoroughly characterized is St. Helena Bay. Shared characteristics of Monterey Bay and St. Helena Bay include: (1) upwelling flows separate from the coast and extend across mouth of bay, creating distinct zones and sharp frontal boundaries; (2) retention inshore of the upwelling plumes favor stratification and development of dinoflagellate blooms, and retention is evident during both upwelling and relaxation; (3) intensity of the dinoflagellate blooms is strongly influenced by physical concentration mechanisms. In Monterey Bay, drifter and model studies indicate that strong nearshore poleward currents develop within and adjacent to the bay during wind relaxation/reversal (unpublished results), suggesting a potential similarity to St. Helena Bay, however none of the limited Monterey Bay drifter observations were made during red tide bloom periods. Due to limited observations, definitive differences between the dinoflagellate ecology of these systems are less certain. One apparent difference is that while red tide is

primarily a relaxation-period phenomenon in St. Helena Bay, the present study shows that red tide can persist in Monterey Bay through upwelling and relaxation. Another apparent difference is that while blooms are transported poleward and retained within St. Helena Bay during relaxation, our study shows significant bloom flushing from Monterey Bay during relaxation. Some key comparative aspects are simply unexplored. For example, dinoflagellates accumulate in the frontal zone across the mouth of St. Helena Bay during upwelling, but studies in Monterey Bay have not specifically sampled fronts to evaluate this possibility.

5. Conclusions

Coastal areas having the conditions that generate frequent intense blooms, such as northern Monterey Bay, may disproportionately influence the greater coastal marine ecosystems in which they reside. Subject to rapid changes in circulation that result from synoptic weather patterns, such “bloom incubators” may serve as seed sources to adjacent coastal environments. Identification of particularly active bloom sites and understanding of coastal transport patterns are prerequisite for determining where in situ monitoring resources are most needed. Emergent coastal ocean observing systems are essential to advance this challenging research area that has significant implications for ecosystem and human health.

Acknowledgments

This research was supported by the David and Lucile Packard Foundation and by NASA grant NAG5-12692 and is part of the GEOHAB Harmful Algal Blooms in Upwelling Systems Core Research Project. We thank MBARI AUV operations for acquisition of the AUV data, and the MBARI Observatory Support Group for mooring support. M0 mooring data were provided by the Center for Integrated Marine Technology under NOAA award NA160C2936. MODIS Level 1 data were provided by the Level 1 and Atmosphere Archive and Distribution System (LAADS), and our MODIS data processing was enabled by the NASA MODIS Ocean Biology Processing Group and the NASA SeaDAS software development team. We thank the AVIRIS and MAS sensor teams, Dryden Flight Research Center and the ER-2 pilots for the airborne remote sensing used in this study. We thank K. Buck for assistance with the phytoplankton data.

References

Anderson, D.M., 1995. Toxic red tides and harmful algal blooms: a practical challenge in coastal oceanography. Reviews of Geophysics 33(suppl.), 1189-1200.

Anderson, D.M., Pitcher, G. C., Estrada, M., 2005. The comparative systems approach to HAB research. Oceanography 18, 148-157.

Asner, G.P., Green, R.O., 2001. Imaging Spectroscopy Measures Desertification in United States and Argentina. EOS 82(49): 601-606.

Barber R.T., Smith, R.L., 1981. Coastal upwelling ecosystems, p. 31-68. In Longhurst, A.R. (Ed.), Analysis of Marine Ecosystems, Academic.

Bolin, R.L., Abbott, D.P., 1963. Studies on the marine climate and phytoplankton of the central coastal area of California, 1954-1960. California Cooperative Oceanic Fisheries Investigations 9:23-45.

Breaker, L.C., Broenkow, W.W., 1994. The circulation of Monterey Bay and related processes. Oceanography and Marine Biology: An Annual Review 32:1-64.

Broenkow, W.W., Smethie, W.M., 1978. Surface circulation and replacement of water in Monterey Bay. Estuarine and Coastal Marine Science 6:583-603.

Broenkow, W.W., and Breaker, L.C., 2005. A 30-year history of tide and current measurements in Elkhorn Slough, California. Scripps Institution of Oceanography Library. Retrieved July 13, 2007 (http://repositories.cdlib.org/sio/lib/8).

Buck, K.R., Chavez, F. P., Campbell L., 1996. Basin-wide distributions of living carbon components and the inverted trophic pyramid of the central gyre of the North Atlantic Ocean, summer 1993. Aquatic Microbial Ecology 10: 283-298.

Buck, K.R., Marin III, R., Chavez, F.P., 2005. Heterotrophic dinoflagellate fecal pellet

production: grazing of large, chain-forming diatoms during upwelling events in Monterey Bay, California. Aquatic Microbial Ecology 40: 293–298.

Cahill, B., Schofield, O., Chant, R., Wilkin, J., Hunter, E., Glenn, S., Bissett, P., 2008. Dynamics of turbid buoyant plumes and the feedbacks on near-shore biogeochemistry and physics, submitted to Geophys. Res. Let.

Castilla, J.C., Lagos, N.A., Guinez, R., Largier, J.L., 2002. Embayments and nearshore retention of plankton; the Antofagasta Bay and other examples. In Castilla, J.C., Largier, J.L. (Eds.), The Oceanography and Ecology of the Nearshore and Bays in Chile. Proceedings of the International Symposium on Linkages and Dynamics of Coastal Systems: Open Coasts and Embayments, Santiago Chile, 2002. Ediciones Universidad Catolica de Chile, Santiago pp. 179-203.

Cullen, J.J., Horrigan, S.G., 1981. Effects of Nitrate on the Diurnal Vertical Migration, Carbon to Nitrogen Ratio, and the Photosynthetic Capacity of the Dinoflagellate *Gymnodinium splendens*. Marine Biology, 62**,** 81-89.

Curtiss, C.C., Langlois, G.W., Busse, L.B., Mazzillo, F., Silver, M.W., 2008. The emergence of *Cochlodinium* along the California Coast (USA). Harmful Algae 7:337-346.

Dierssen, H.M., Kudela, R.M., Ryan, J.P., Zimmerman, R.C., 2006. Red and black tides: Quantitative analysis of water-leaving radiance and perceived color for phytoplankton, colored dissolved organic matter, and suspended sediments. Limnology and Oceanography 51(6): 2646-2659.

Donaghay, P.L., Osborn, T.R., 1997. Toward a theory of biological-physical control of harmful algal bloom dynamics and impacts. Limnology and Oceanography 42, 1283-1296.

Donaghay, P.L., Sullivan, J.M., Rines, J.E., Graff, J., Hanson, A.K. Holliday, D.V., 2006. The

Importance of Swimming Behavior in Controlling the Formation, EOS 87(36) suppl.

Dugdale, R.C., Wilkerson, F.P., Barber, R.T., Blasco, D., Packard, T.T., 1987. Changes in nutrients, pH, light penetration and heat budget by migrating photosynthetic organisms. Oceanol. Acta, Proceedings International Symposium on Equatorial Vertical Motion, Paris, 6-10 May 1985, p. 103-107.

Eppley, R.W., Reid, F.M.H., Strickland, J.D.H., 1970. Estimates of phytoplankton crop size, growth rates and primary production. Bull. Scripps. Inst. Oceanogr. 17: 33-42.

Fawcett, A., Pitcher, G., Bernard, S., Cembella, A. and Kudela, R., 2007. Contrasting wind patterns and toxigenic phytoplankton in the southern Benguela upwelling system. Marine Ecology Progress Series, 348, 19-31.

Franks, P.J.S., Anderson, D.M., 1992. Alongshore transport of a toxic phytoplankton bloom in a buoyancy current: *Alexandrium tamarense* in the Gulf of Maine. Marine Biology 112,153-164.

Franks, P.J.S., 1997. Spatial patterns in dense algal blooms. Limnol. Oceanogr. 42, 1297-1305.

Franz, B.A., Werdell, P.J., Meister, G., Kwiatkowska, E.J., Bailey, S.W., Ahmad, Z., McClain, C.R., 2006. MODIS Land Bands for Ocean Remote Sensing Applications, Proc. Ocean Optics XVIII, Montreal, Canada, 9-13 October 2006.

Gao, B.C., Montes, M.J., Ahmad, Z., and Davis, C.O., 2000. Atmospheric correction algorithm for hyperspectral remote sensing of ocean color from space. Applied Optics 39:887-896.

GEOHAB. 2005. Global Ecology and Oceanography of Harmful Algal Blooms, GEOHAB Core Research Project: HABs in Upwelling Systems, G. Pitcher, T. Moita, V. Trainer, R. Kudela, P. Figueiras, T. Probyn (Eds.), SCOR and IOC, Paris and Baltimore, 82 pp.

Gower J., King, S., Borstad, G., Brown, L., 2005. Detection of intense plankton blooms using the

709 nm band of the MERIS imaging spectrometer. Int. J. Remote Sensing 26, 2005-2012.

Graham W.M., Field, J.G., Potts, D.C., 1992. Persistent 'upwelling shadows' and their influence on zooplankton distributions. Marine Biology 114, 561-570.

Graham W.M., 1993. Spatio-temporal scale assessment of an 'upwelling shadow' in northern Monterey Bay, California. Estuaries 16, 83-91.

Graham W.M., Largier J.L., 1997. Upwelling shadows as nearshore retention sites: the example of northern Monterey Bay. Continental Shelf Research 17, 509-532.

Heaney, S.I., Eppley, R.W., 1981. Light, temperature and nitrogen as interacting factors affecting diel vertical migrations of dinoflagellates in culture. Journal of Plankton Research, 3(2), 331-344.

Horner, R.A., Garrison, D.L., Plumley, F.G., 1997. Harmful algal blooms and red tide problems on the U.S. West coast. Limnology and Oceanography 42, 1076-1088.

Johnson, K.S., Coletti, L.J., 2002. In situ ultraviolet spectrophotometry for high resolution and long term monitoring of nitrate, bromide and bisulfide in the ocean. Deep-Sea Research I 49, 1291-1305.

Kahru, M., Mitchell, B.G., Diaz, A., Miura, M., 2004. MODIS Detects a Devastating Algal Bloom in Paracas Bay, Peru. EOS, Trans. AGU 85: 465-472.

King, M.D., Menzel, W.P., Grant, P.S., Myers, J.S., Arnold, G.T., Platnick, S.E., Gumley, L.E., Tsay, S.C., Moeller, C.C., Fitzgerald, M., Brown, K.S., Osterwisch, F.G., 1996. Airborne scanning spectrometer for remote sensing of cloud, aerosol, water vapor and surface properties. J. Atmos. Oceanic Technol. 13, 777-794.

Kudela, R., Pitcher, G., Probyn, T., Figueiras, F., Moita, T., Trainer, V., 2005. Harmful Algal Blooms in coastal upwelling systems. Oceanography 18, 184-197.

Kudela, R.M., Ryan, J.P., Blakely, M.D., Lane, J.Q., Peterson, T.D., 2008. Linking the physiology and ecology of *Cochlodinium* to better understand harmful algal bloom events: a comparative approach. Harmful Algae, *7*, 278-292.

Letelier, R.M., Abbott, M.R., 1996. An Analysis of Chlorophyll Fluorescence Algorithms for the Moderate Resolution Imaging Spectrometer (MODIS). Remote Sens. Environ. 58, 215-223.

Moita, M.T., Palma, S., Oliviera, P.B., Vidal, T., Silva, A., Vilarinho, M.G., 2006. The return of Gymnodinium catenatum after 10 years: bloom initiation and transport of the Portuguese coast. Proceedings of 12th International Congress on Harmful Algae, PO.06-14, September 2006, Copenhagen.

Narvaez, D.A., Poulin, E., Leiva, G. Hernandez, E., Castilla, J.C., Navarrette, S.A., 2004. Seasonal and spatial variation of nearshore hydrographic conditions in central Chile. Continental Shelf Research 24: 279-292.

Pennington J.T., Chavez, F.P., 2000. Seasonal fluctuations of temperature, salinity, nitrate, chlorophyll and primary production at station H3/M1 over 1989-1996 in Monterey Bay, California. Deep-Sea Research II 47, 947-973.

Pitcher, G.C., Nelson, G., 2006. Characteristics of the surface boundary layer important to the development of red tide on the southern Namaqua shelf of the Benguela upwelling system. Limnology and Oceanography 51, 2660-2674.

Ramp, S.R., Paduan, J.D., Shulman, I., Kindle, J., Bahr, F.L., and Chavez, F.P., 2005. Observations of upwelling and relaxation events in the northern Monterey Bay during August 2000. J. Geophys. Res. 110, C07013, doi:10.1029/2004JC002538.

Reid, J.L., Roden, G.I., Wyllie, J.G., 1958. Studies of the California Current System. California Cooperative Oceanic Fisheries Investigations, Progress Report, 1 July 1956 – 1 January

1958, pp. 27-56.

Rienecker, E.R., Ryan, J.P., Marin III, R., Blum, M., Dietz, C., Chavez, F.P., 2008. Synoptic mapping of the phytoplankton size distribution, with applications to the ecology of red tides and harmful algal blooms, Limnology and Oceanography: Methods 6, 153-161.

Rosenfeld, L.K., Schwing, F.B., Garfield, N., Tracy, D.E., 1994. Bifurcated flow from an upwelling center: a cold water source for Monterey Bay. Continental Shelf Research 14:931-964.

Ryan, J.P., Dierssen, H.M., Kudela, R.M., Scholin, C.A., Johnson, K.S., Sullivan, J.M., Fischer, A.M., Rienecker, E.V., McEnaney, P.R., Chavez, F.P., 2005. Coastal ocean physics and red tides: an example from Monterey Bay, California. Oceanography 18, 246-255.

Ryan, J.P., McManus, M.A., Paduan, J.D., Chavez, F.P., 2008a. Phytoplankton thin layers in Monterey Bay, California. Marine Ecology Progress Series, 354, 21-34.

Ryan, J.P., Gower, J.F.R., King, S.A., Bissett, W.P., Fischer, A.M., Kudela, R.M., Kolber, Z., Mazzillo, F., Rienecker, E.R., Chavez, F.P., 2008b. A coastal ocean extreme bloom incubator. Geophysical Research Letters, accepted.

Ryther, J.H. 1955. Ecology of autotrophic marine dinoflagellates with reference to red water conditions. Pp. 387-414 in The Luminescence of Biological Systems, F. H. Johnson, ed, AAAS, Washington.

Ryther, J.H., 1969. Photosynthesis and fish production in the sea. Science 166, 72-76.

Schalles, J.F., 2006. Optical remote sensing techniques to estimate phytoplankton chlorophyll a concentration in coastal waters with varying suspended matter and CDOM concentrations. In: Richardson, L.L., LeDrew, E.F. (Eds.), Remote Sensing of Aquatic Coastal Ecosystem Processes: Science and Management Application, Springer, Chapter 3.

Skogsberg, T., 1936. Hydrography of Monterey Bay, California. Thermal conditions, 1929-1933. Transactions of the American Philosophical Society 90, 350-386.

Skogsberg, T., Phelps, A., 1946. Hydrography of Monterey Bay, California. Thermal conditions, Part II 1934-1937. Proceedings of the American Philosophical Society 90, 350-386.

Smayda, T.J., 1997. Harmful algal blooms: their ecophysiology and general relevance to phytoplankton blooms in the sea. Limnology and Oceanography 42, 1137-1153.

Smayda, T.J., 2000. Ecological features of harmful algal blooms in coastal upwelling systems. South African Journal of Marine Science 22, 219-253.

Smayda, T.J., 2002. Turbulence, watermass stratification and harmful algal blooms: an alternative view and frontal zones as pelagic seed banks. Harmful Algae 1, 95-112.

Sournia, A., 1995. Red-tide and toxic marine phytoplankton of the world ocean: an inquiry into biodiversity. In: Lassus, P., Arzul, G., Erard-Le Denn, E., Gentien, P., Marcaillou-LeBaut, C. (Eds.), Harmful Marine Algal Blooms. Lavoisier, Paris, pp. 103-112.

Stegmann, P.M., Foley, D.G., King, C., Schwing, F.B., Price, H., Bograd, S.J., Palacios, D.M., 2006. Integrating enhanced satellite data maps into coastal management. EOS 87(14):137.

Stumpf, R.P., Litaker, R.W., Lanerolle, L., Tester, P.A., 2008. Hydrodynamic accumulation of Karenia off the west coast of Florida. Continental Shelf Research 28, 189-213.

Tester, P.A., Stumpf, R.P., Vukovich, F.M., Folwer, P.K., Turner, J.T., 1991. An expatriate red tide bloom: transport, distribution, and persistence. Limnology and Oceanography 36, 1053-1061.

Figure Captions

Figure 1. Climatological SST for the study computed from August – October, 2002 – 2007 MODIS SST. Upwelling centers are at Point Año Nuevo and Point Sur. Moorings at stations M0 and M1 provided meteorological and oceanographic data used in this study. M0 is on the northern shelf in 75 m water depth; M1 is over Monterey Submarine Canyon in 1000 m water depth. Surface phytoplankton samples were taken at station C1 and mooring M1 during the study.

Figure 2. Methods to quantify bloom intensity from multi-spectral remote sensing. The centers of sensor measurement bands used in the remote sensing algorithms are marked by triangles for MODIS chlorophyll fluorescence line height (FLH), MERIS maximum chlorophyll index (MCI), and MODIS Airborne Simulator (MAS) bloom index (BI). For each sensor, only the three bands covering the spectral range of chlorophyll fluorescence and bloom red/NIR reflectance, i.e. those used for bloom imaging, are shown. Band widths differ between bands on the same sensor, and between the multispectral sensors. The two reflectance spectra are from in situ measurements in Monterey Bay on September 21-22, 2006, using a Satlantic Profiler II. Note that the peak near 700 nm rises and shifts to longer wavelengths at higher chlorophyll concentrations.

Figure 3. (a) Chlorophyll and water mass changes measured at mooring M0. Shown are chlorophyll at 2 m, and the average of salinity measured at 3.5, 10 and 20 m. The hourly time series were 33-hour low-pass filtered to exclude diurnal and tidal signals. (b) 33-hour low pass filtered winds at mooring M1 during the bloom expansion and dispersion period. The times of MODIS images presented in Figure 4 are marked by diamonds and vertical lines.

Figure 4. Description of bloom development from satellite remote sensing. Images are true-color, fluorescence line height (FLH) and sea surface temperature (SST) images from the MODIS satellite sensor, and the maximum chlorophyll index (MCI) from the MERIS satellite sensor. Vectors represent ADCP-measured velocity at 20 m depth at mooring M1, and in the depth range 10-20 m at mooring M0, averaged over the 24 hour period preceding each image. The base of each vector is at the mooring location; a reference vector of 25 cm s^{-1} is shown in (a). Numbers in (d) and (e) identify features described in the text. Image times are shown relative to the mooring observations in Figure 3.

Figure 5. High-resolution airborne remote sensing of bio-optical and physical conditions during a critical phase of bloom expansion. a) SST and b) bloom Index (BI) are from MODIS Airborne Simulator (MAS) imaging on August 26, 2004. Vectors in (a) represent ADCP-measured velocity at 20 m depth at mooring M1, and in the depth range 10-20 m at mooring M0, averaged over the 24-hour period preceding image acquisition. The base of each vector is at the mooring location; a reference vector of 25 cm s^{-1} is shown in (a). The white lines show the transects made by the AUV on August 26-27 (see Figure 7). The inset of (b) shows the peak reflectance wavelengths of the red tide bloom in the far red – near infrared, measured concurrently by AVIRIS.

Figure 6. Illustration of bloom advection from high-temporal-resolution airborne remote sensing. MAS SST and bloom Index (BI) images were taken ~ 1 hour apart on August 26. Arrows serve as fixed spatial references. The sequence illustrates movement of bloom waters

northward near shore (arrow 1) and southward along the inshore edge of the upwelling filament (arrow 2). The white contour is the 16.25°C isotherm.

Figure 7. Observation of bloom transport made by autonomous underwater vehicle (AUV). AUV transect locations are shown in Figure 5a. The daytime survey on August 26 was from the northern transect (a,b); during the subsequent night a survey was run along the southern line (c,d). Both AUV surveys progressed from onshore to offshore, sampling between 2 m and near-bottom; only the depth range 2 to 20 m is shown. High phytoplankton abundance is indicated by shading, relative to temperature (contours in top panels) and nitrate (contours in bottom panels).

Table 1. Statistics of phytoplankton biomass for autotrophic dinoflagellates and diatoms at time-series stations C1 and M1 (summed) during the dinoflagellate red tide bloom period. See methods for description of biomass estimates.

	17 August	**8 September**
Dinoflagellate biomass (µg C L^{-1})	556	1667
Diatom biomass (µg C L^{-1})	246	34
Dinoflagellate/diatom biomass ratio	2.3	49

Figure 1

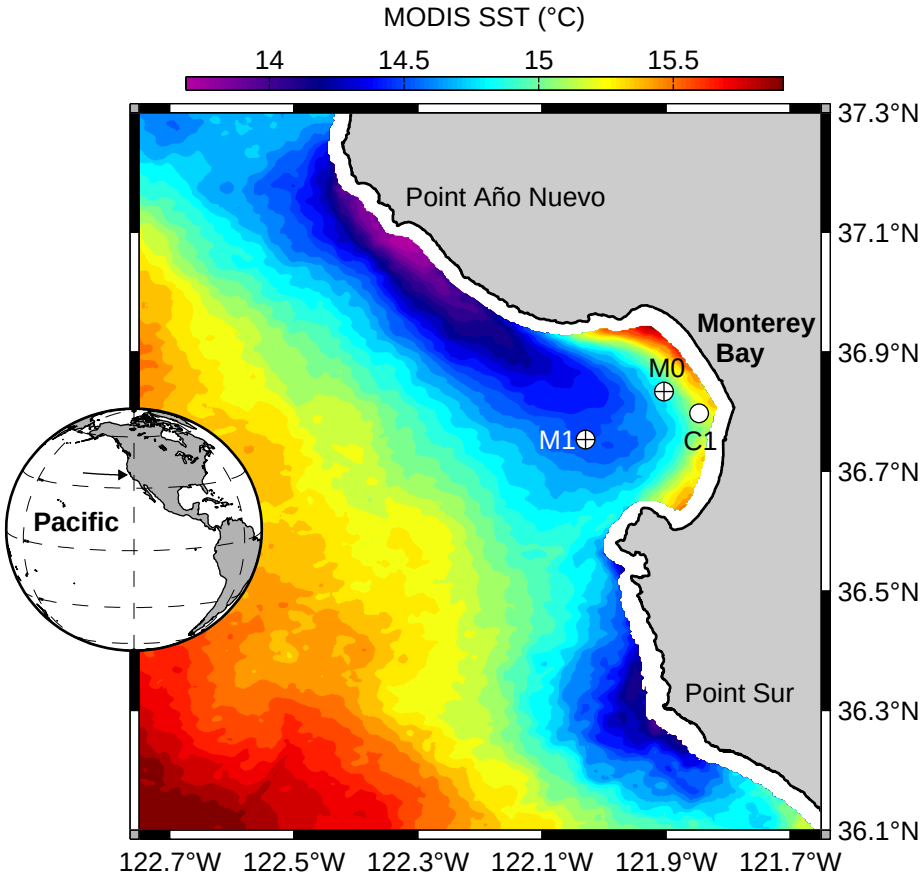
MODIS SST (°C)
14
14.5
15
15.5
Point Año Nuevo
Monterey
Bay
M0
M1
C1
Point Sur
Pacific
37.3°N
37.1°N
36.9°N
36.7°N
36.5°N
36.3°N
36.1°N
122.7°W
122.5°W
122.3°W
122.1°W
121.9°W
121.7°W

Figure 2

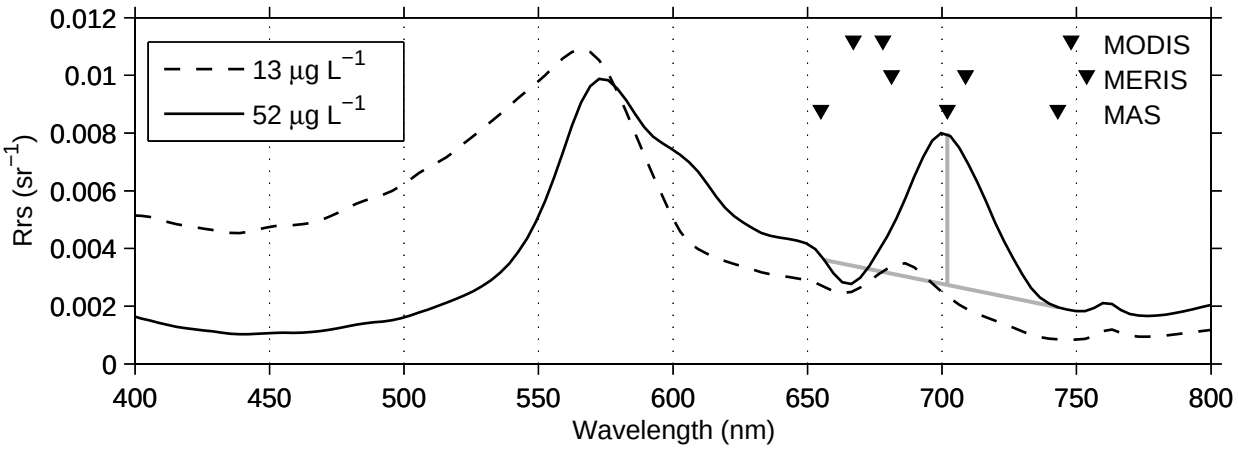
0.012
0.01
0.008
0.006
0.004
0.002
0
Rrs (sr^{-1})
13 µg L^{-1}
52 µg L^{-1}
MODIS
MERIS
MAS
400
450
500
550
600
650
700
750
800
Wavelength (nm)

Figure 3

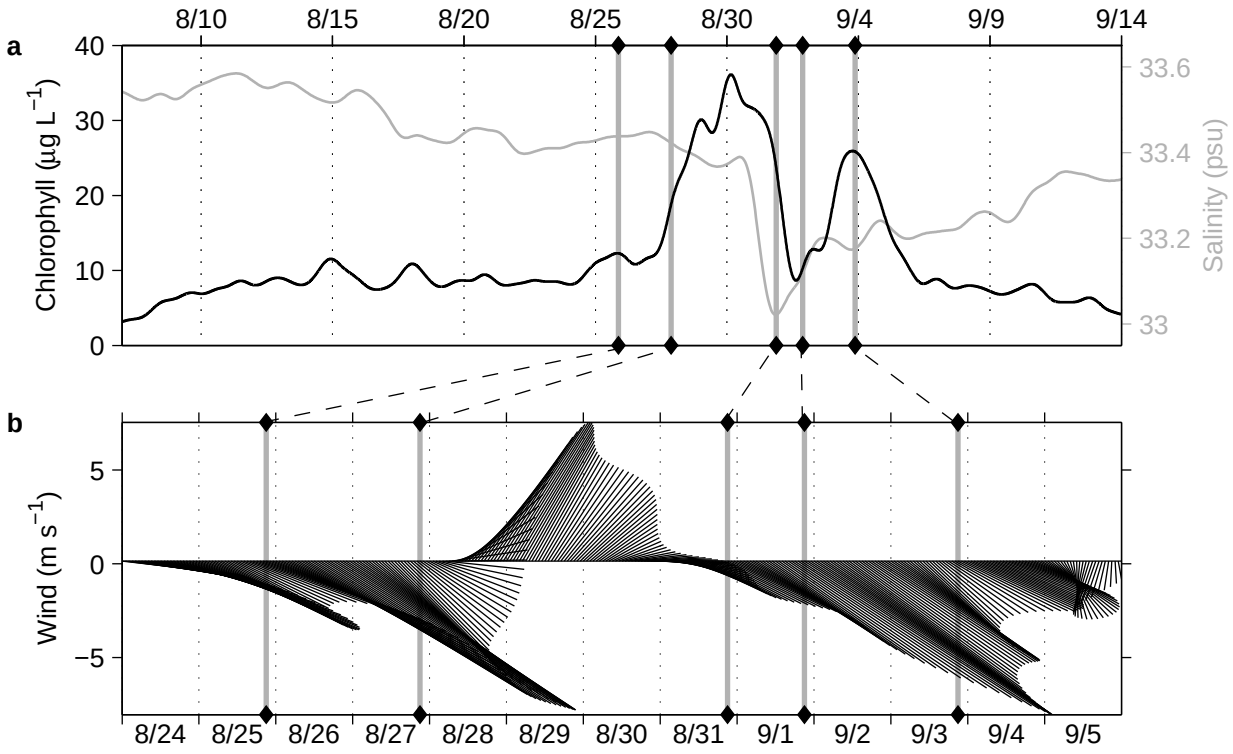
a
b
8/10
8/15
8/20
8/25
8/30
9/4
9/9
9/14
Chlorophyll (µg L^{-1})
Salinity (psu)
Wind (m s^{-1})
8/24
8/25
8/26
8/27
8/28
8/29
8/30
8/31
9/1
9/2
9/3
9/4
9/5

Figure 4

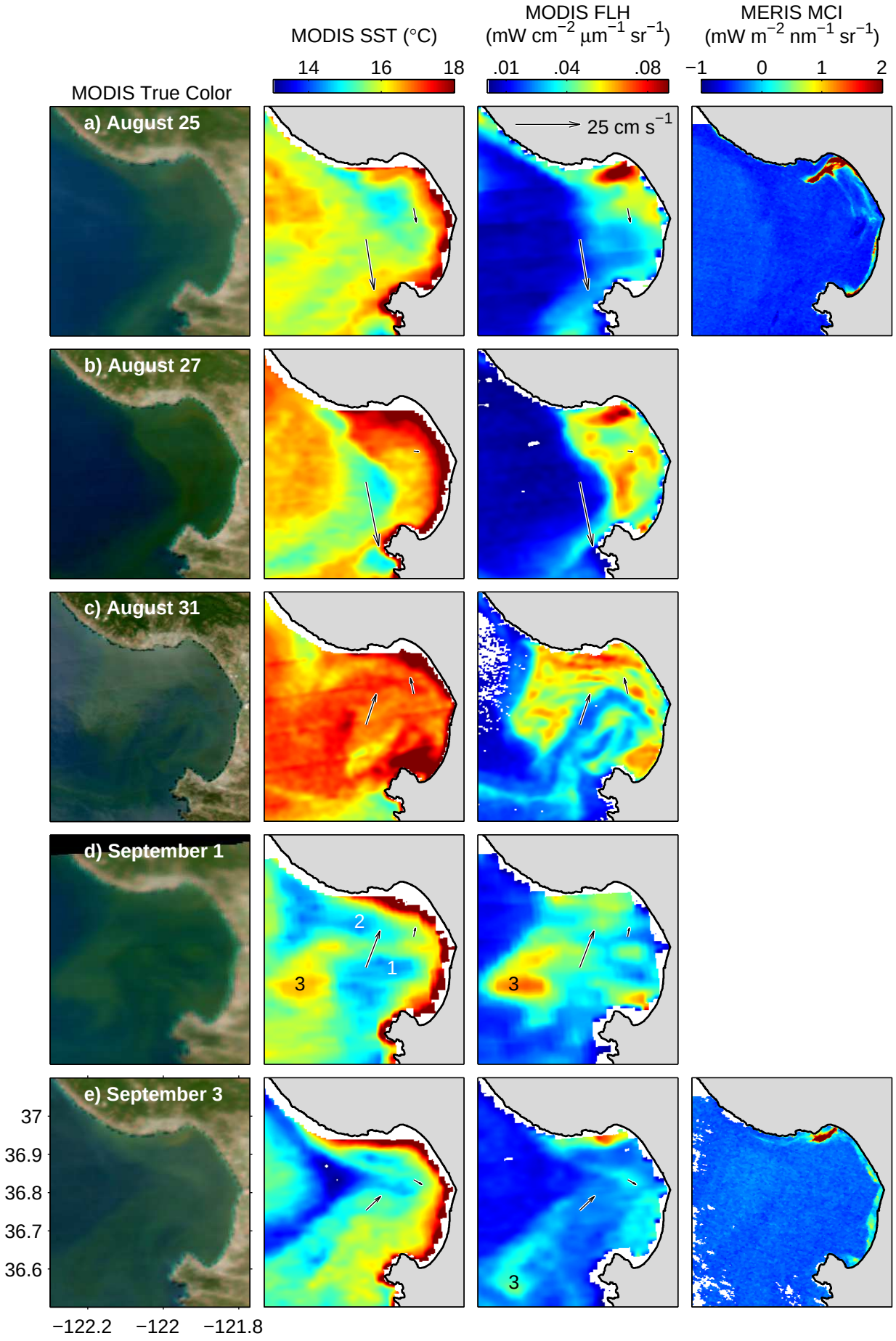
MODIS True Color
MODIS SST (°C)
14
16
18
MODIS FLH
(mW cm^{-2} µm^{-1} sr^{-1})
.01
.04
.08
MERIS MCI
(mW m^{-2} nm^{-1} sr^{-1})
−1
0
1
2
a) August 25
25 cm s^{-1}
b) August 27
c) August 31
d) September 1
1
2
3
3
e) September 3
3
37
36.9
36.8
36.7
36.6
−122.2
−122
−121.8

Figure 5

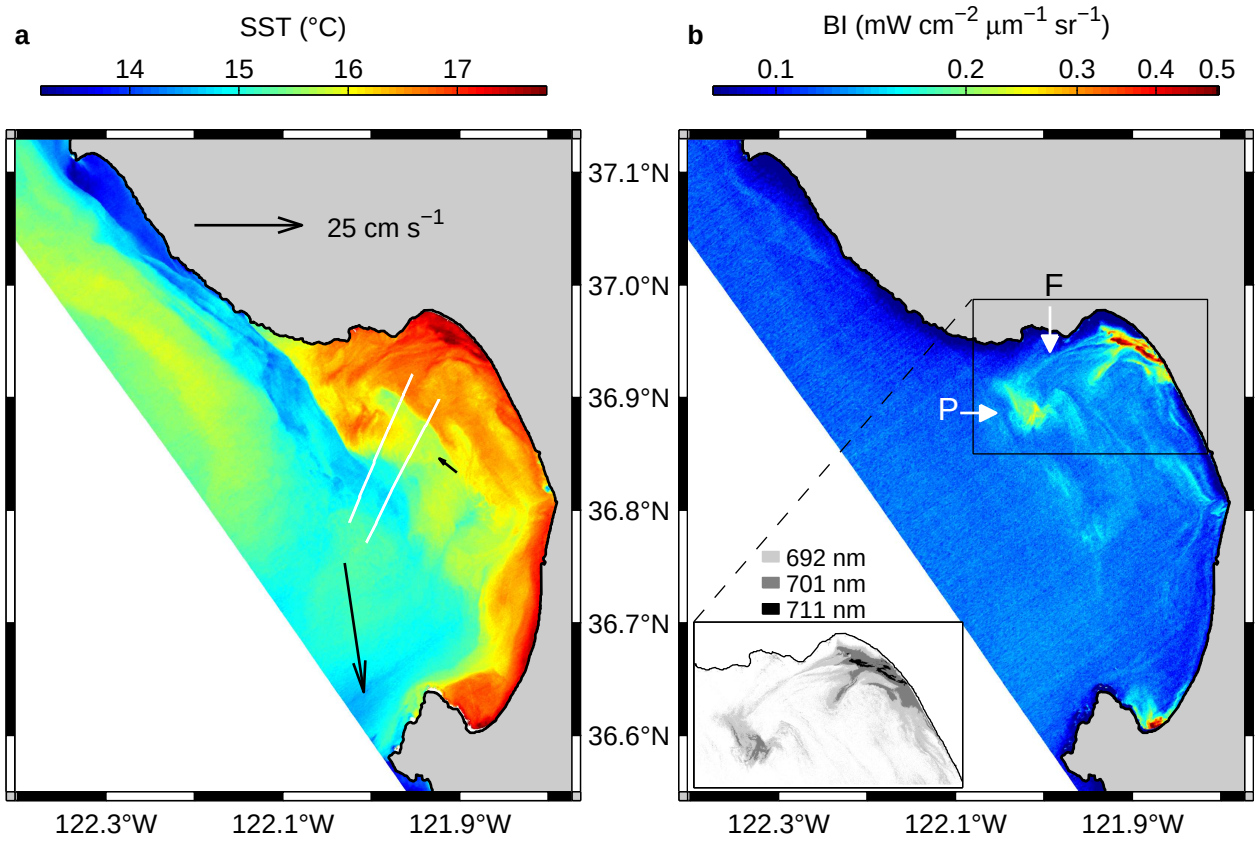
a
SST (°C)
14
15
16
17
25 cm s−1
b
BI (mW cm−2 µm−1 sr−1)
0.1
0.2
0.3
0.4
0.5
F
P
692 nm
701 nm
711 nm
37.1°N
37.0°N
36.9°N
36.8°N
36.7°N
36.6°N
122.3°W
122.1°W
121.9°W
122.3°W
122.1°W
121.9°W

Figure 6

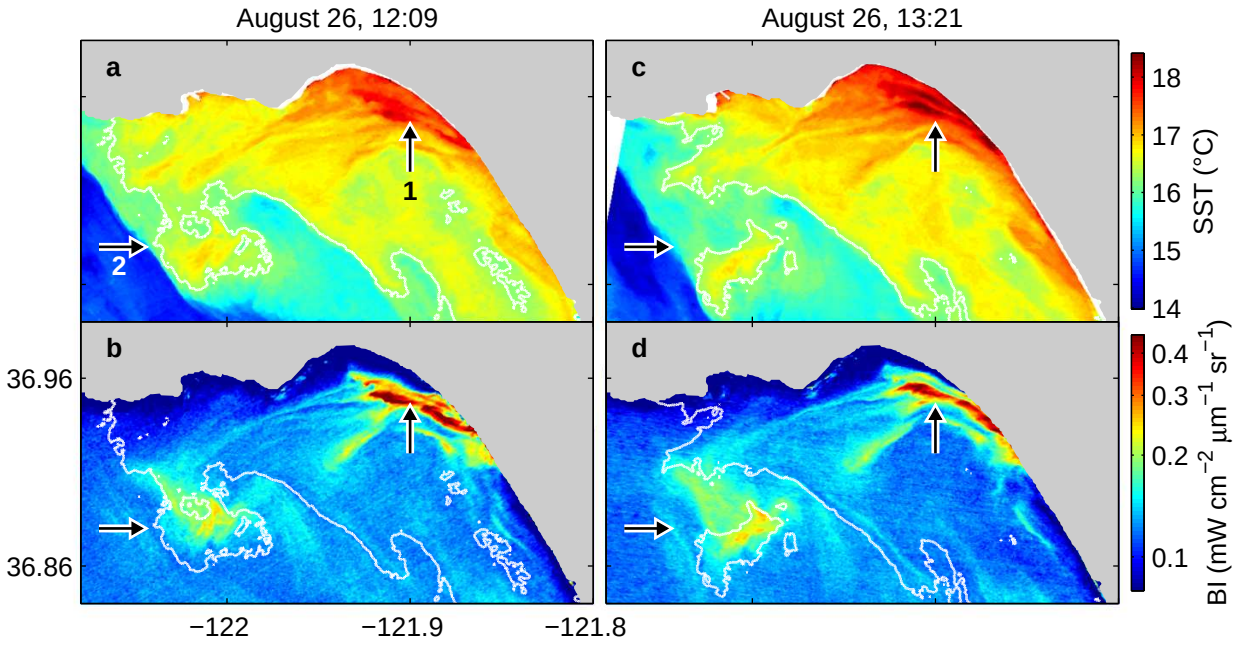
August 26, 12:09
August 26, 13:21
a
b
c
d
1
2
36.96
36.86
−122
−121.9
−121.8
18
17
16
15
14
SST (°C)
0.4
0.3
0.2
0.1
BI (mW cm^{-2} μm^{-1} sr^{-1})

Figure 7

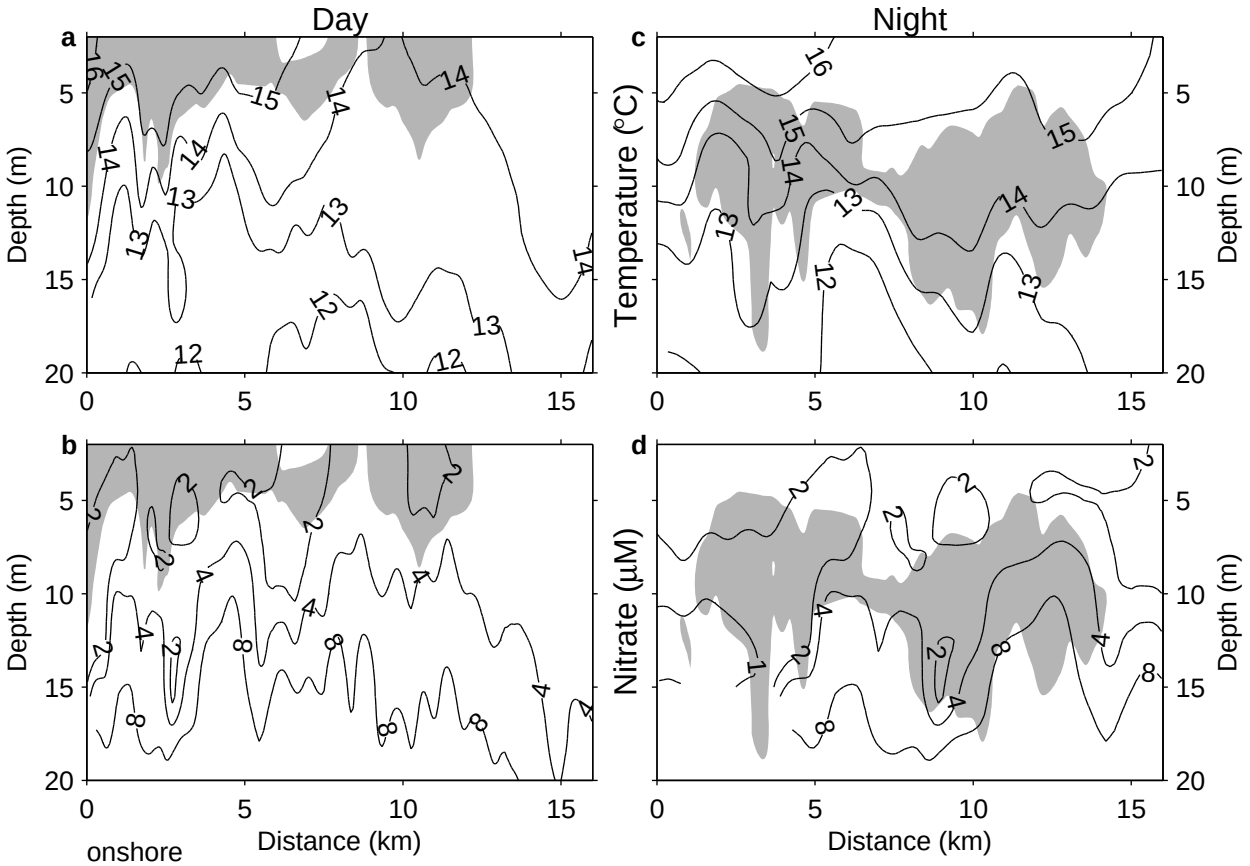
Day
Night
a
b
c
d
Depth (m)
Temperature (°C)
Nitrate (µM)
Distance (km)
onshore